The Pennsylvania State University

The Graduate School

IN-SITU MONITORING OF POWDER FLOW IN DIRECTED ENERGY DEPOSITION ADDITIVE MANUFACTURING

A Thesis in

Mechanical Engineering

by

Baily Thomas

Submitted in Partial Fulfillment
of the Requirements
for the Degree of

Master of Science

August 2021

The thesis of Baily Thomas was reviewed and approved by the following:

Abdalla Nassar
Head of Process Physics, Analytics, and Engineering Department
Associate Research Professor Applied Research Laboratory
Thesis Advisor

Timothy W. Simpson
Paul Marrow Professor of Engineering Design and Manufacturing
Faculty Reader

Karen Thole
Department Head and Distinguished Professor, Mechanical Engineering

ABSTRACT

Powder-fed directed energy deposition (DED) additive manufacturing (AM) is useful for the repair and production of high-value, metal parts. The simultaneous production of a material and geometric features, however, presents several challenges. Among these challenges are the large number of processing parameters, interdependence between parameters, and the effect of component design and orientation on resulting microstructure, geometry, and properties. In-situ monitoring of DED parameters provides the opportunity to measure the effects of processing parameters and identify process anomalies. One primary processing parameter, which is rarely monitored in-situ, is the powder flow. The powder flow of a DED system significantly effects part quality, including geometrical inaccuracy and defect formation.

During DED, systemic variation in powder flow (e.g., caused by changes in carrier gas, purge gases, or nozzle geometry) along with anomalous variations (e.g., caused by obstructions at the nozzle exits) occur. These variations are, however, difficult to monitor during the DED process. This study provides a solution for detection of both systemic and anomalous variations through the use of an in-situ powder flow monitoring (PFM) system. A calibration method is developed for direct, spatially-resolved measurement of mass flow rate at the nozzle exit. The use of the developed PFM system, calibration methods, and data analysis enables two- and three-dimensional mapping of powder flow on an inter-layer basis during DED and is demonstrated for detection of systemic and anomalous flow variations. By reducing the occurrences of these variations as well as monitoring for in-process error, increased levels of manufacturing consistency and confidence can be achieved.

TABLE OF CONTENTS

LIST OF FIGURES

LIST OF TABLES

ACKNOWLEDGEMENTS

This effort was funded under Rolls-Royce Corporation Research Agreement A19-0049 titled "Sensor-based Quality Monitoring of Directed Energy Deposition Additive Manufacturing."

Chapter 1

Introduction

Additive manufacturing (AM) is now widely used within the aerospace and defense industries for production of high-value components [1]. While there exist many technologies under the umbrella of AM, one of the primary metal AM technologies that is increasingly integrated into industry is directed energy deposition (DED). The advantages of DED are fast build speeds, flexible build envelope, and lower cost compared to other AM techniques [2]. The DED process is also widely used for not only part production but also repair [2].

Use of AM, in general, and DED, in particular, requires consideration of process parameter selection, material selection, build orientation and post processing. Process parameter selection, typically based on experimental design of experiments [3, 4] and sometimes augmented with physics-based models [5], is complicated by the interdependent nature of AM processing parameters. Experimentally-driven “black box” testing, where the effect of an input variable is tested via deposition followed by post-process inspection and iteration, is inefficient, expensive, and often misses variable interactions and variations. In-situ sensing technologies offers the potential to directly observe the effects and interactions of input variables, reducing the need for “black box” testing and enabling near-real-time quality control.

One processing parameter that directly affects the resulting deposition [6] and is a source of both systemic and anomalous error [7] is the powder flow. Powder flow results in systemic error through unoptimized nozzle geometry and processing parameters. Powder flow experiences anomalous error through powder feeder failures (e.g., clogs, flow inconsistencies, nozzle obstruction). While powder flow monitoring systems have been implemented into DED AM, an *in-situ monitoring technique for post nozzle exit powder flow has yet to be explored in order to solve both systemic and anomalous error*.

This work focuses on in-situ monitoring of DED powder flow. The predominate characteristics of powder flow that affect build quality are feed rate, convergence distance, powder capture efficiency, and variations due to systemic and anomalous error. The purpose of this study is to develop and demonstrate monitoring methods capable of directly measuring these characteristics. A corollary objective is identification of systemic and anomalous error during DED processes.

These efforts are accomplished through the use of a camera and laser-line system capable of z-axis adjustment within the build chamber. The developed powder flow monitoring (PFM) system is capable of characterizing the flow shape and powder intensity utilizing 2D and 3D mapping of individual powder particles. System calibration enables analysis of both bulk and local powder flow rates. Visualization and quantitative analysis of the powder flow under several use cases (e.g., varying process parameter, characterization of nozzle damage, and in-process monitoring of powder flow variability) demonstrate the value of the developed methods. Adoption of the developed in-situ PFM methods enables rapid observation, and potentially correction of, systemic and anomalous variations in powder flow during DED of high-value components.

In the next chapter, the current state of the art regarding DED and powder flow sensing will be discussed. This includes the gaps which this study’s developed sensor can fill. In Chapter 3, the methodology for both the calibration and use cases will be laid out according to the flowchart determined early in the study. Chapter 4 will discuss the results of both the calibration and the multiple use cases. Finally, Chapter 5 will state our conclusions from this study as well as future work which could further aid in the improvement of DED AM process confidence.

Chapter 2

Literature Review

In laser-based, powder-fed DED, metal powders are introduced into a melt pool formed by the laser melting of a substrate. Typical laser types used in this process include Nd: YAG solid state, Fiber, and CO2 laser [8]. The laser beam and resulting melt pool is then translated across the substrate, which produces a solidified track. Tracks are deposited with a partial overlap upon neighboring tracks to produce an initial layer of a desired part or repair. Layers are then deposited atop previous layers to produce a 3D structure. Laser power, translation speed, and the amount of powder introduced into the melt pool dictate the overall melt pool geometry and subsequently dictate solidified track geometry and microstructure. However, while the translation speed and laser power can be easily monitored and adjusted, there are few well-established methods for monitoring powder flow in-situ.

Primary parameters that influence powder flow characteristics are nozzle geometry, purge gas flow rate, carrier gas flow rate, and powder feed rate. For DED AM, two types of nozzles exist for the introduction of metal powders to the meltpool. These include 4-nozzle systems and coaxial nozzles. A 4-nozzle system divides the powder stream equally among 4 inlets within the deposition head, which then exit from separate nozzles. This system requires precise installation of all four nozzles in order to attain a symmetric powder flow and a uniform focal point based on the angles of the four nozzles. The coaxial nozzle introduces the powder to a chamber with a large amount of inlet holes in a circular formation. These inlet holes lead to the nozzle tip where the powder uniformly exits the nozzle in a circular pattern at some specified angle based on the nozzle geometry.

The nozzle geometry is the primary determining factor for the focus location; however, carrier and purge gas can have an effect as well [9]. Purge gas is implemented in order to ensure that the laser optic remains clean within the deposition column, while the carrier gas is used for the transfer of powder from the hopper to the nozzles. Inert gas (e.g., argon) is utilized for both purge and carrier gas to maintain an inert processing atmosphere. Detailed nozzle design and the selection of purge and carrier gas settings have a profound effect on powder stream characteristics. For instance, a shortened powder convergence distance, which is achieved through a more obtuse angle between nozzles, or an increased exit angle of the powder flow, and reducing gas-flow rate can produce a better powder capture efficiency [9]. A higher capture efficiency results in an increased number of particles which converge at the working distance and are incorporated in the laser interaction zone. This produces an ideal deposition track with minimal wasted powder in the build chamber. However, other studies show that when increasing the gas flow rate, a shorter angle and larger powder convergence distance can be advantageous due to the increased particle velocity and the reduced effects of turbulence on the powder flow [9]. Once configured, nozzle geometry and gas flow rates remain unchanged for a given machine and DED process. Typically, total, time-averaged powder feed rate (i.e., the total powder flowing out of a nozzle over a period of time on the order of minutes) is also assumed constant during deposition.

Total time-averaged powder feed rate is the simplest powder flow parameter to characterize and has been found to impact the resulting thickness and porosity of deposited layers. Achieving a desired solidified layer thickness is necessary to ensure dimensional accuracy. The powder flow rate’s effect on layer thickness as compared to other process parameters’ impacts was determined in a study by Choi et al. [6] utilizing analysis of variance (ANOVA). Parameters of interest were powder flow rate, laser power, and scan speed. The powder flow rate’s effect on the layer thickness error was found to be the strongest and most statistically significant (p-value of 0.0001), whereas the laser power and scan speed were not statically significant (p-value of 0.5160 and 0.1068, respectively) [6]. The effect of powder flow rate on porosity generation was also found to be statistically significant (p-value of 0.0001), while those of laser power and scan speed were not [6]. Interestingly, while higher powder flow was found to enable more precise layer thickness, it also increased porosity. While not directly addressed by Choi et al. [6], it can nevertheless be deduced that variations of powder flow during deposition will have a significant impact on both geometry and porosity within built components.

The total powder flow rate also affects the partitioning of laser power absorption within the laser-interaction zone [10]. In a study by Jhang et al. [10], it was determined that as the powder flow rate of a DED system increases, the absorption of laser power increases within the powder and decreases within the substrate; this is attributed to a shielding effect. As the concentration of powder upstream of the substrate increases, so does the percentage of laser power absorbed within the powder. Correspondingly, less powder makes its way to the substrate below. The results of Jhang et al. [10] are consistent with Choi et al. [6]: an increase in powder flow increases laser absorptivity within the powder, resulting in a thicker layer, likely with less melting in the underlying substrate and correspondingly a higher probability of porosity.

Despite the assumption of a constant powder feed rate, the actual feed rate during the course of a deposition can vary [11]. The degree of variation is partially dependent on the type of powder feeder utilized. A screw feeder utilizes a central, rotating shaft which picks up powder for delivery within the feed lines. Depending on the powder feeder configuration and the desired flow rate, screw feeders can have a wide range of precision [12]. However, more sophisticated powder feeding systems exist that apply various techniques to improve flow rate stability. This includes the use of a rotary disc pickup system under an inert gas pressure [13]. This system increases the powder flow rate precision by increasing the rotational speed of the disc which has a designated number of inlet holes for powder pick up.

Another sophisticated powder feed system is the Oerlikon 9MP [14], which utilizes air-driven vibration coupled with variable pressure differentials in order to adjust the powder feed rate. This system also takes advantage of feedback control in order to adjust the pressure and achieve the desired powder flow. Along with various powder feed system delivery methods, some powder feeders also allow for mixing of various powders. These systems use multiple powder containers which enter a powder blender before carrier gas transfers powder to the deposition head [6].

Few studies have been undertaken to assess variations or oscillations in the powder feed rate. Preliminary work by Brown, et al. [15], however, has demonstrated that significant oscillation in powder flow rate can occur using rotary disc pickup feeders. Using a target powder flow rate of 2 grams per minute (gpm) of Inconel 625 powder, a measured oscillation frequency on the order of 0.054 Hz (~18.5 s period) was observed—see Figure 2-1. Such fluctuation is likely to impact resulting component geometry and quality.

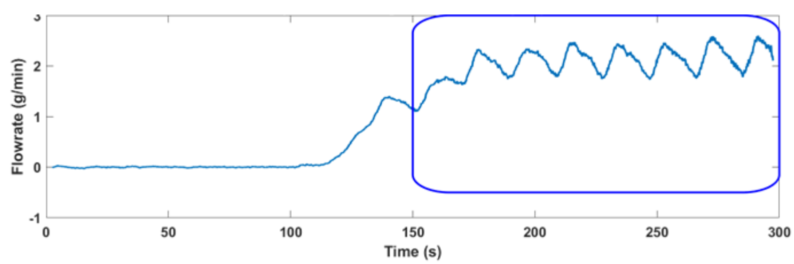

Figure **2-1**: Assessment of powder flow fluctuations using scale measurements. Used with permission from [15]

In contrast to flow rate fluctuations, flow (i.e., stream) geometry has been more thoroughly investigated, typically for model validation. The primary method for characterization of flow geometry utilizes a laser light source to illuminate the powder stream and a camera to image the flow geometry [9, 16]. Similar data were also collected through the use of a thermal camera [17]. This method produces a 2D visual of the powder flow, which can aid in characterizing the shape of the powder flow distribution. This can be used for determining if the flow parameters cause flow turbulence, which reduces the powder retention in the meltpool. A representative image is shown in Figure 2-2.

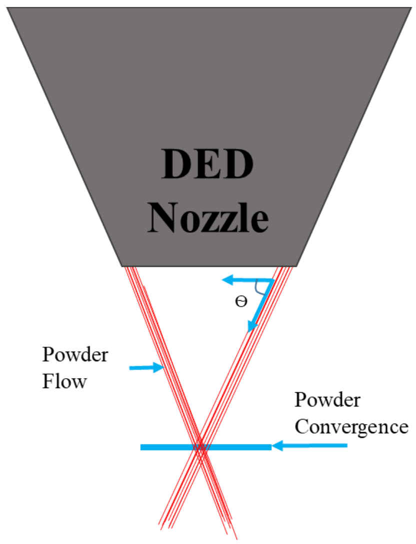

Figure **2-2**: Powder flow convergence and angle of exit for coaxial nozzle

Illuminated imaging of the powder stream has also been applied for characterization of the working distance of a powder deposition head. Making use of the laser illumination source and high-speed camera sensing, the focus location of any particular nozzle/nozzles can be characterized and improved upon to attain a desired powder concentration [9, 10, 18, 19, 20]. This improvement is based on experimentally varying the gas flow rate and redesigning the nozzle to attain a particular result, such as a higher powder capture efficiency. While these sensing technologies and techniques are useful to characterize and improve the powder flow, they are also limited in their inability to provide real-time, quantitative data for process monitoring or control. Rather, the primary purpose for these imaging methods is to validate computational fluid dynamics (CFD) simulations [6, 9, 10, 16, 17, 18, 19].

In-situ monitoring of powder flow often utilizes single-point detectors (e.g., photodiodes, acoustic sensors). One example is the implementation of a laser and photo diode within the powder feeding system. A laser diode directs light, through a glass window into the powder stream as it travels to the deposition head, which is received by a photo diode [21]. This method analyzes the powder flow rate with a high level of accuracy which can be used in feedback control loops for a powder feed system. Because sensing occurs at a single point in the powder stream, any inconsistencies further downstream or at the nozzle outputs are not captured.

Another sensing technology that performs a similar analysis is the use of acoustic emissions (AE). Vibrations resulting from powder flow within feed lines are correlated to measured powder flow and enable detection of variability on the order of 10% [11]. This type of system suffers from the same restriction as photodiodes in that it is only indicative of the flow rate at a specific location within the feed lines.

The current gap in the literature regarding in-situ, quantitative powder flow rate monitoring post nozzle exit is apparent, i.e., the lack of post nozzle, real time flow data. This study attempts to close this gap through the development of a powder flow monitoring (PFM) system together with a calibration procedure. The PFM system is demonstrated through multiple use cases. The use cases include the detection of powder variability due to process parameter variation, nozzle damage, and in-process error. The goal of applying these use cases to the developed PFM system is ultimately to increase the confidence in the system to detect error through both experimental data and improved process parameter development methodologies.

In the next chapter, the methodology of this study is discussed. This includes the methods for the sensor set up, calibration, and the sensor utilized in various use cases. These methods lay the foundation for the development of a robust, multifunctional sensing technology.

Chapter 3

Methods

A key consideration for powder flow monitoring of a DED AM system is the location of the monitoring system. While other studies have analyzed flow within the powder feed lines [11, 21], this work focuses on monitoring the flow post nozzle exit, at and above the working distance. This location is of interest because variations in both powder feed rate and powder stream characteristics (e.g., geometry, density) directly above the melt pool can be assessed. The location is thus the most informative on systemic and anomalous powder flow variation.

In this work, three-steps were used to develop and implement a powder flow monitoring (PFM) system: development of the sensing technology, the generation of robust calibration metrics, and technology demonstration through three use cases (see Figure 3-1).

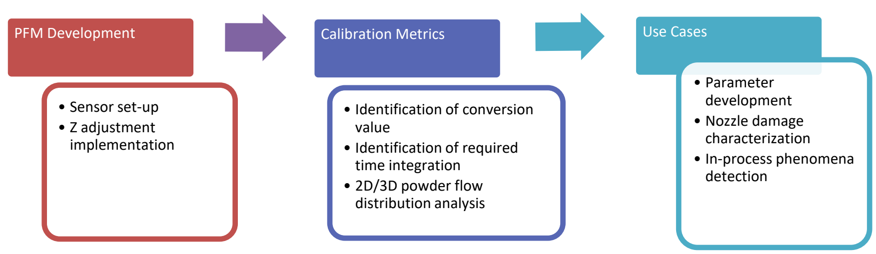

Figure **3-1**: Research flowchart

Directed Energy Deposition System

In this study, two DED AM machines were utilized. The first machine used was a commercial Optomec LENS MR-7 DED machine equipped with an IPG Photonics Yb-doped fiber laser with a max laser power of 500W. Processing parameters (laser power, powder flow rate, processing speed, and carrier/purge gas flow rates) were optimized for the building of test blocks for the study of the powder flow. An Oerlikon 9MP [14] powder feeder, equipped with an air-driven vibrator and weight-based, closed-loop monitoring and control of the feed rate was used together with the Optomec LENS MR-7. The powder used on this machine was Inconel 718 sieved with mesh sizes -170/+325 with a D50 size of 69.9 µm. Argon was used for both the carrier gas and purge gas.

Experiments were conducted using both the nominal Optomec LENS 4-nozzle deposition head as well as a third-party, coaxial nozzle deposition head. The nominal 4-nozzle head, shown in Figure 3-2, contained four radially symmetrically powder-delivery nozzles, each with an exit orifice diameter of 1.2 mm. Each nozzle was oriented at 18.25º with respect to the laser propagation direction. A center purge nozzle, which provided shielding argon gas, was 6.35 mm in diameter.

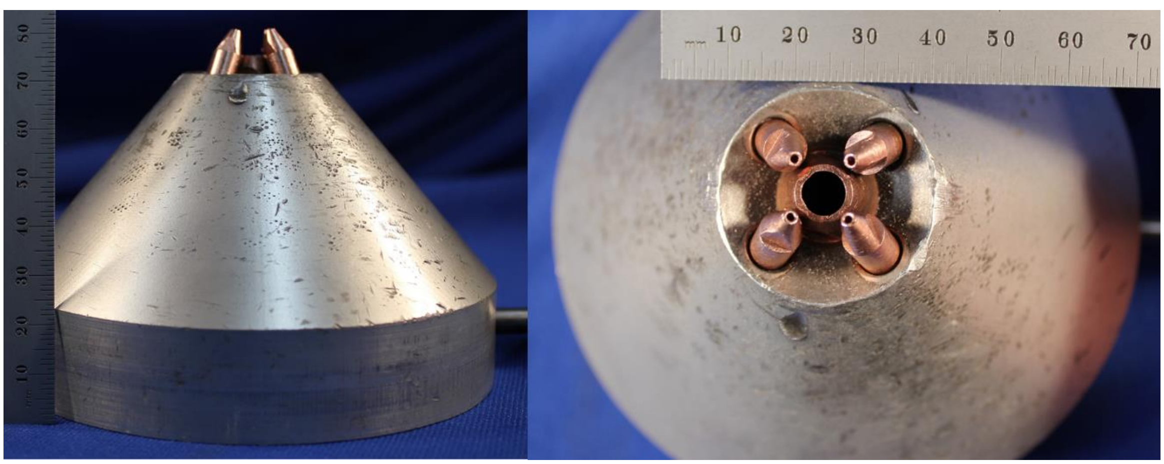

Figure **3-2**: Nominal Optomec LENS 4-nozzle3 deposition head

The third-party, coaxial nozzle utilized was a 1.55 mm inner radial orifice surrounded by a 2.7 mm outer radial orifice, resulting in a 0.8 mm wide hollow, cylindrical exit for the powder.

The nozzle exit angle was ~16º relative to the laser propagation direction, with a total nozzle height of ~42 mm. The nozzle also had damage to the tip from previous processing including overall damage to the nozzle tip shape as shown in Figure 3-3.

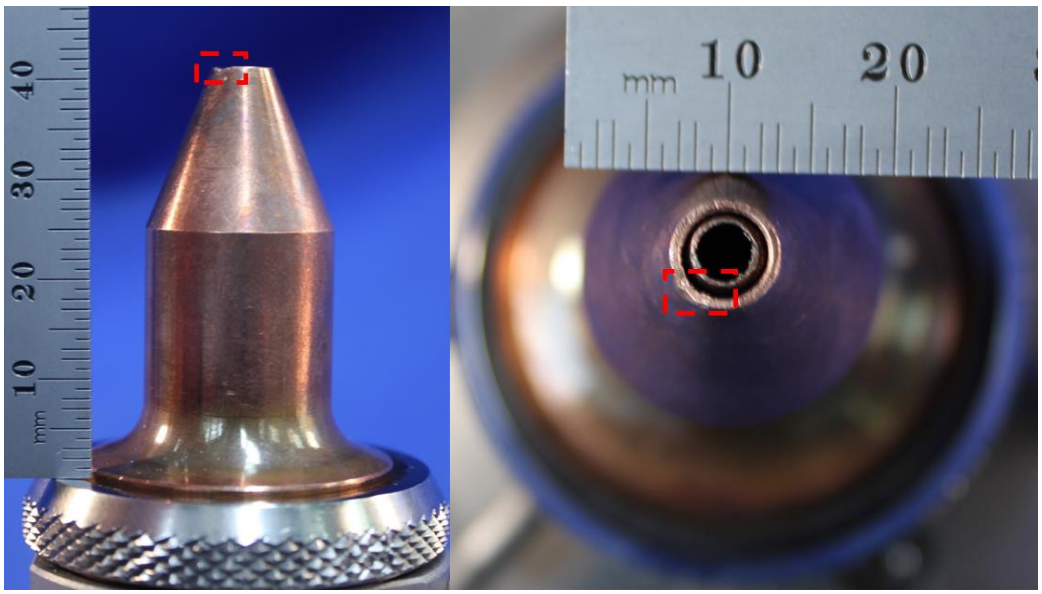

(a) (b)

Figure **3-3**: Commercial coaxial nozzle integrated into Optomec LENS MR-7 with highlighted damaged on the nozzle tip.

The second machine used was a DMG Mori Lasertec 65 equipped a disc powder feeder, including a powder feed rate sensor and automatic powder feed calibration. A total of three coaxial nozzles were used for powder flow rate analysis. The first two nozzles used were an undamaged and a damaged nozzle both with a 3 mm inner radial orifice surrounded by a 5 mm outer radial orifice, resulting in a 0.36 ± 0.059 mm wide hollow, cylindrical exit for the powder. The nozzle exit angle was 20º relative to the laser propagation direction, with a total nozzle height of ~49 mm. The damaged nozzle shows visible error in the gap spacing of +0.02 mm and -0.17 as shown in Figure 3-4. Each of these nozzles utilized 316L stainless steel powders with mesh sizes -140/+352.

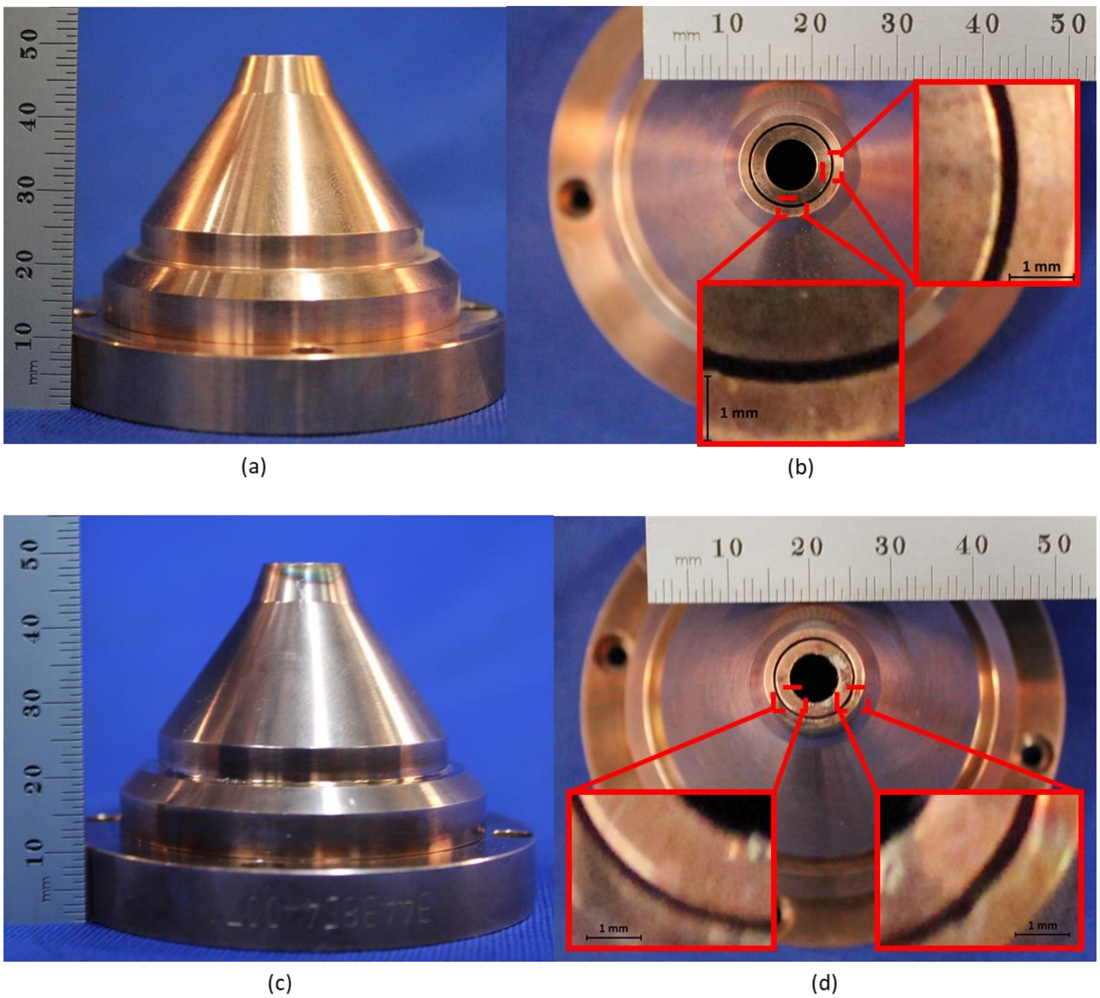

Figure **3-4**: 3 mm coaxial nozzle on DMG Mori Lasertec 65 (a) undamaged side view, (b) undamaged nozzle, (c) damaged side view, and (d) damaged nozzle

While the first two nozzles were solely used for powder flow analysis, the third nozzle was used to compare the powder flow characteristics to a resulting line deposit. The processing parameters utilized for the resulting deposit used in this study are shown in Table 3-1.

Table **3-1:** Processing parameters for 1.6 mm coaxial nozzle within DMG Mori Lasertec 65

Laser power	Travel speed	Carrier gas	Center purge gas	Powder feed rate	Working Distance
1000 W	39.4 IPM	4 L/min	3 L/min	1.5 g/min	7.5 mm

The third nozzle was a damaged nozzle with a 1.6 mm radial inner orifice, surrounded by a 2.8 mm outer radial orifice, resulting in a 0.18 mm wide hollow, cylindrical exit for the powder. The nozzle exit angle was 20º relative to the laser propagation direction, with a total nozzle height of ~54 mm. The nozzle damage is shown in Figure 3-5 where a visible dent is present which constricts the gap to 0.03-0.14 mm. Powder utilized with this nozzle was Scalmalloy with mesh size -140/+352.

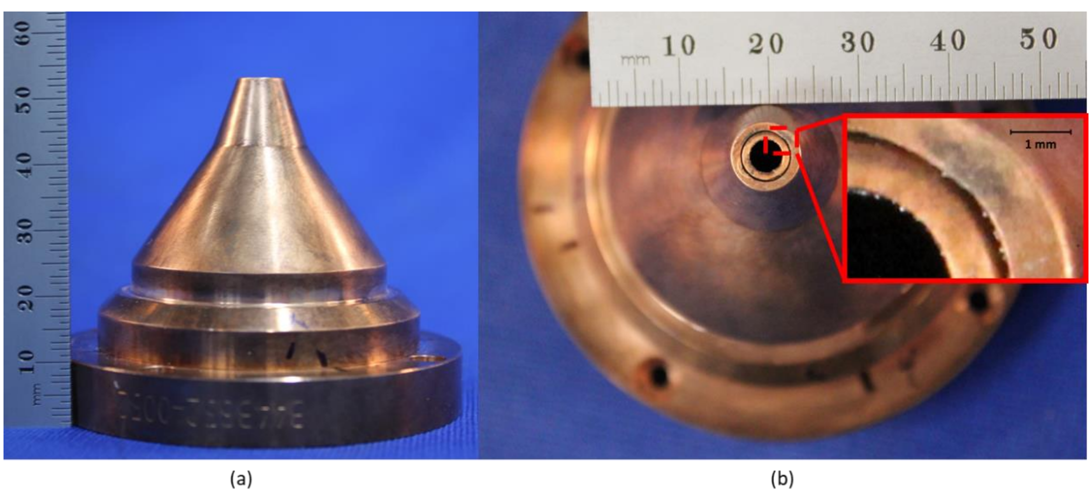

Figure **3-5**: 1.6 mm coaxial nozzle on DMG Mori 65 (a) side view and (b) top view

In total, four different configurations were utilized in this study. Each configuration, in order of appearance for Chapter 4, is shown in Table 3-2 with its respective system, nozzle, powder, and application.

Table **3-2**: Nozzle/machine configurations with their corresponding powder used and application

Config.	System	Nozzle	Powder	Application
1	Optomec LENS MR-7	4-nozzle	Inconel 718	PFM calibration
2	DMG Mori Lasertec 65	Undamaged/damaged coaxial nozzles	316L SS	Flow shape comparison
3	DMG Mori Lasertec 65	Damaged coaxial nozzle	Scalmalloy	Correlation to resulting deposit
4	Optomec LENS MR-7	Damaged coaxial nozzle	Inconel 718	Spatter build up analysis

PFM Sensor Configuration

Powder flow, post nozzle exit, was assessed via laser-line illumination coupled with a high-speed camera integrated into the chamber of a DED system. The experimental setup consisted of a fixture that rigidly housed the laser line and high-speed camera systems. The laser line was rigidly oriented perpendicular to the powder flow, illuminating an x-y plane in the build chamber space. The high-speed camera was rigidly oriented at a 25˚ angle toward the laser-line plane to produce a “viewing window” on the illuminated x-y plane. The laser line was placed so that the powder flow from the nozzle passed through the laser line roughly at the center. The laser-line and camera were attached to a motorized, linear stage, along the z axis, parallel to the powder flow, so that the laser line was able to pass through any location of interest along the powder focusing region. This experimental set up is shown in Figure 3-6 Here, the laser line, camera, and translation stage are referred to as the PFM sensor.

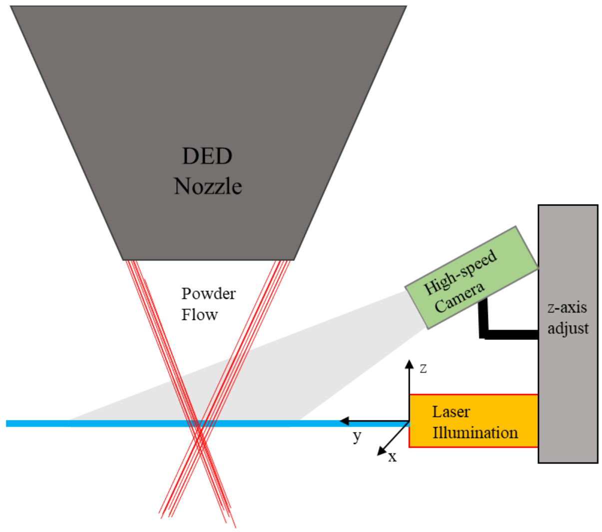

Figure **3-6**: Camera and laser illumination experimental setup on coaxial nozzle

As the powder particles pass through the laser line, they become illuminated briefly. Using the high-speed camera, the moment in time at which a powder particle is illuminated is recorded as well as its position within the laser line's x-y plane. Utilizing a LabVIEW program, the transformed x-y coordinates of each particle (i.e., bright pixel) and the time associated with each frame are stored in a SQLite database (.db) file. Each data point, with its corresponding x-y position, and time data, is denoted as a detection of a powder particle. The cumulative total of powder particles within a frame divided by the frame integration time (~50 us) represents the instantaneous powder flow rate.

At typical powder flow rates (~1 – 4 gpm), the number of particles sampled within a single frame are too low for representative sampling; therefore, sampling over multiple frames is necessary. In this work, a frame rate of ~1.5 kHz (1 sample per 1500 us), and an integration time of 60 us were used. An integration time less than the time between successive frames results in a gap in data collected, as shown in Figure 3-7. This gap results in sampling roughly 12% of the flow. In order to account for this gap, a conversion value is determined from powder particle detections to a powder flow rate (gpm).

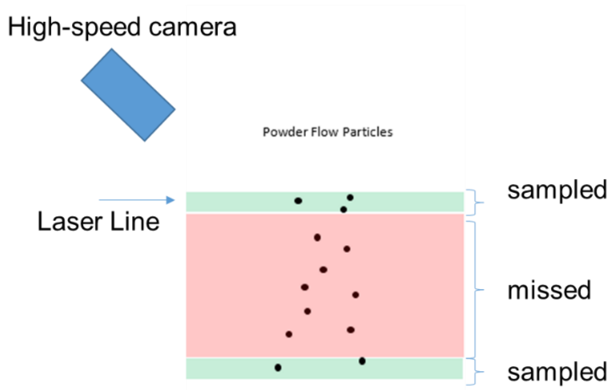

Figure **3-7**: Monitoring system data collection gap.

Correlation between PFM Detection and Mass Flow Rate

The correlation between measured powder flow rate and the number of powder particle detections was determined by simultaneously measuring the mass of powder exiting the nozzle/nozzles over a one-minute period with a high precision scale and the number of particle detections with the PFM sensor. The high precision scale was integrated into the build chamber of the machine in order to collect the powder directly beneath the illumination plane of the PFM sensor. To capture all particles exiting the DED deposition head, a powder trap was used to collected particles atop the scale (see Figure 3-9).

A linear function was used to correlate the PFM sensor detection and the scale-measured mass flow rate. The correlation coefficient and coefficient of determination (R^2) were initially determined using 25 one-minute tests at varying powder flow rates utilizing 4 nozzles, as shown in Figure 3-8. For the coaxial nozzle on the LENS MR-7 system, 10 one-minute tests with a consistent powder flow rate of 1.2 g/min were performed. In this work, a correlation coefficient and coefficient of determination were only determined for configurations (1) and (4) on the LENS MR-7 system. The measured R^2 values for configuration (1) and (4) were 0.9977 and 0.9863, respectively. These excellent correlations between measured mass and PFM detections show that time between successive imaging frames does not contribute significant error.

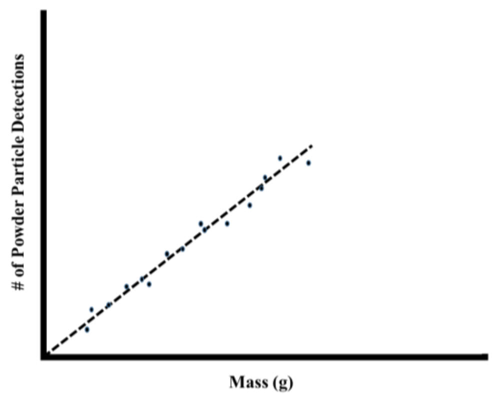

Figure **3-8**: Powder flow rate graph to determine correlation.

Minimum PFM Sampling Time

To determine the minimum number of frames necessary (i.e., minimum PFM sampling time) to accurately predict mass flow rate values, the instantaneous correlation between the powder particle detections and the mass was assessed. This was achieved through the use of a high-precision scale ($\pm$0.01 grams) which, communicating with a LabVIEW program, recorded the cumulative mass of flowing powders with respect to time. A data acquisition rate of ~1 Hz was used. A powder trap aided in directing powder particles to the scale. The experimental setup is shown in Figure 3-9.

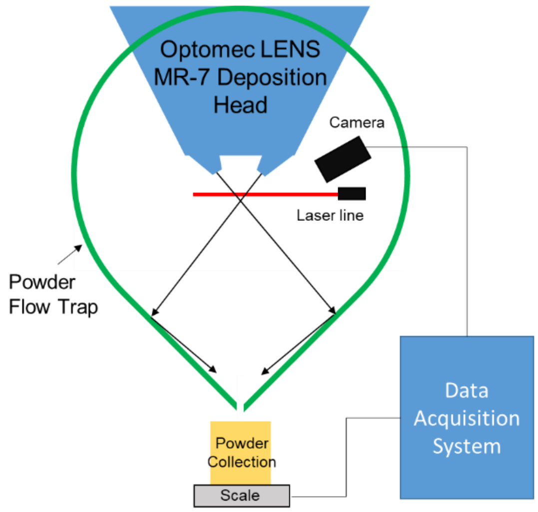

Figure **3-9**: Scale and monitoring system integration setup.

In order to obtain a minimum time required to produce representative data using the PFM system, the cumulative scale-measured and cumulative PFM-measured powder mass were compared. The derivative of each of these data sets represents the instantaneous PFM-measured $\left(\frac{\Delta \text{detetction} \times \text{Corr.Coeff}}{\Delta t}\right)$ and scale-measured $\left(\frac{\Delta m}{\Delta t}\right)$ powder flow rates, respectively. Due to the high acquisition rate of the PFM sensor (~1.5 kHz), compared with the mass scale (1 Hz), significant fluctuations were observed in PFM detection with a sampling time (Δt) of less than 0.67 ms. Increasing the sampling time, in increments of 5 ms, reduced fluctuations in the PFM and scale-measured powder flow rates. A minimum PFM sampling time of 15 ms resulted in an acceptable reduction of noise and a fit between the PFM-measured and scale-measured powder flow rates and was determined sufficient for all flow rates of interest.

In-plane Powder Distribution (2D Analysis)

Powder flow over a given x-y plane was visualized using intensity heatmaps. A heatmap is a data visualization tool where a color gradient is applied to depict the intensity of the powder flow within a region, as shown in Figure 3-10, where the color transitions from blue (low intensity) to red (high intensity). The heatmap is indicative of the powder focus region where the highest concentration of powder particles is in the center while the powder particle intensity reduces with increasing distance from the center.

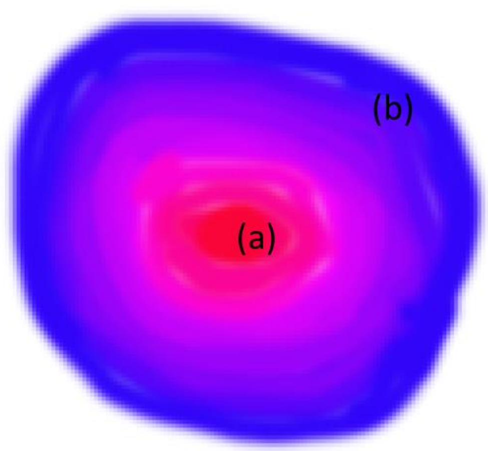

Figure **3-10**: Intensity Heatmap

This visualization of the powder flow in 2D is determined by using the powder particle detections location in the x-y plane over a time period. The heat map can be used qualitatively, or quantitatively in conjunction with mass flow rate data, to both inform a user of the consistency of the overall powder flow as well as the specific locations in the x-y plane where flow uniformity varies. In this work, 2D heatmaps are generated using the PFM-measured number of particle detections. Each particle, from the set of particle $\{p_i\}_{i=1}^{n}$, has an associated location of each detection (x_i, y_i). For ease of analysis, particle locations are converted from Cartesian into polar coordinates (r_i, θ_i), equations 1 and 2.

$$r_i = \sqrt{(x_i - x_0)^2 + (y_i - y_0)^2} \tag{1}$$

$$\theta_i = \begin{cases} arctan\left(\frac{y_i - y_0}{x_i - x_0}\right), & x \geq 0 \; and \; y > 0) \\ arctan\left(\frac{y_i - y_0}{x_i - x_0}\right) + \pi, & x < 0 \; and \; y \geq 0 \\ arctan\left(\frac{y_i - y_0}{x_i - x_0}\right) + \pi, & x \leq 0 \; and \; y < 0 \\ arctan\left(\frac{y_i - y_0}{x_i - x_0}\right) + 2\pi, & x > 0 \; and \; y \leq 0 \end{cases} \tag{2}$$

The center of the plot $(r = 0)$ is chosen at the centroid of all detected particles (x_0, y_0), shown in equation 3.

$$\mathrm{x}_0 = \frac{\sum \mathrm{x_i}}{\mathrm{n}} \;,\; \mathrm{y}_0 = \frac{\sum \mathrm{y_i}}{\mathrm{n}} \tag{3}$$

Once converted into polar coordinates as shown in Figure 3-7, the mass flow rate over a range of radii and angles is determined by multiplying the correlation coefficient by the sum of all particles, captured within a one second period, which satisfy the ranges of $r\epsilon\ [r_{min}, r_{max}]$, $\theta\epsilon[\theta_{min}, \theta_{max}]$. Using particle detection locations in polar coordinates, a best-fit Gaussian distribution $(f(x, \mu, \sigma) = \frac{1}{\sigma\sqrt{2\pi}} e^{\frac{-(x-\mu)^2}{2\sigma^2}})$ was applied. This distribution was chosen due to the uniform powder scattering observed surrounding the highest powder concentration for planes above the powder convergence. The same distribution was also applied at the powder convergence, however a different distribution, Weibull or Chi-Squared, may produce better results. We define the effective powder flow radius (r_{eff}) as the mean of a best-fit Gaussian distribution to the number of particle detections over all angles $(\theta\epsilon\ [0, 2\pi])$.

The powder flow envelope is defined by the standard deviation (STD) of the Gaussian fit, such that the powder flow envelope is defined as between $[r_{eff} - \sigma, \mathrm{r_{eff}} + \sigma]$. For a coaxial nozzle, the powder envelope thickness (2σ) is illustrated as the effective width (w_{eff}) of the powder flow. An illustration of a Gaussian fit and calculation of r_{eff} and the (w_{eff}) is provided in Figure 3-11.

Powder uniformity, as a function of polar angle, is determined by comparing the mean (r_{eff}) and standard deviation (w_{eff}) from finite ranges of angles. A significant variation of mean values as a function of polar angle is indicative of restrictions, obstructions, or irregularity in powder flow.

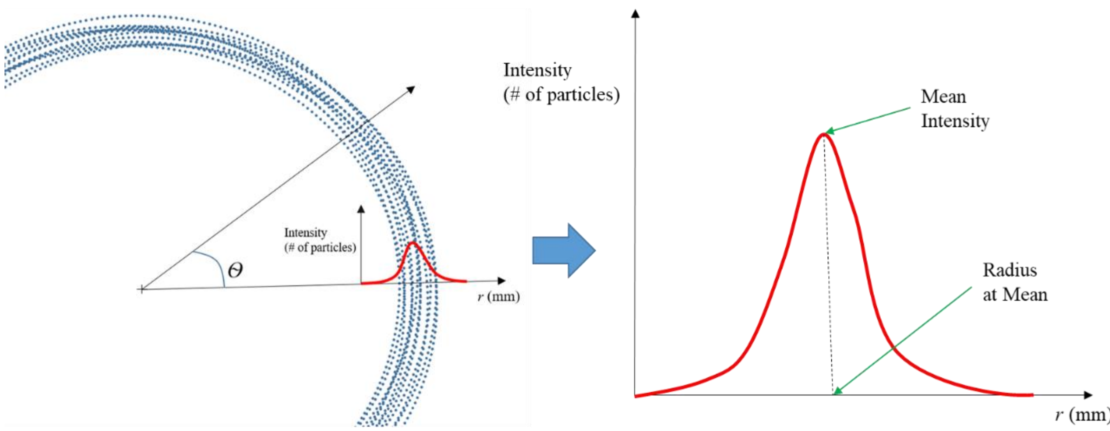

Figure **3-11**: Gaussian distribution of powder flow intensity based on theta

3D Analysis

Translation of the PFM system along the z-axis, using an automated stage allows 3D analysis of the powder flow. At each z-location, the 2D analysis is applied to determine the effective powder stream envelope as a function of propagation distance $(r_{eff}(z))$. For this work, 10 scans were taken on the Optomec LENS MR-7 while 30 scans were taken on the DMG-Mori, both along the z-axis, starting just below the nozzle and ending past the powder focus location. To achieve this, each z-step was 0.5 mm with each scan consisting of 5 seconds of data collection. Data for each z-step were stored in individual SQLite (.db) files, and later combined in MATLAB to produce a 3D visualization of the powder flow. This methodology is illustrated in Figure 3-12 for the in-process monitoring use case on the Optomec LENS MR-7, where 10 sets of PFM data, at 10 z-locations, were used to produce a 3D visualization of the powder flow. The average time required for data collection inter-layer is ~1 minute.

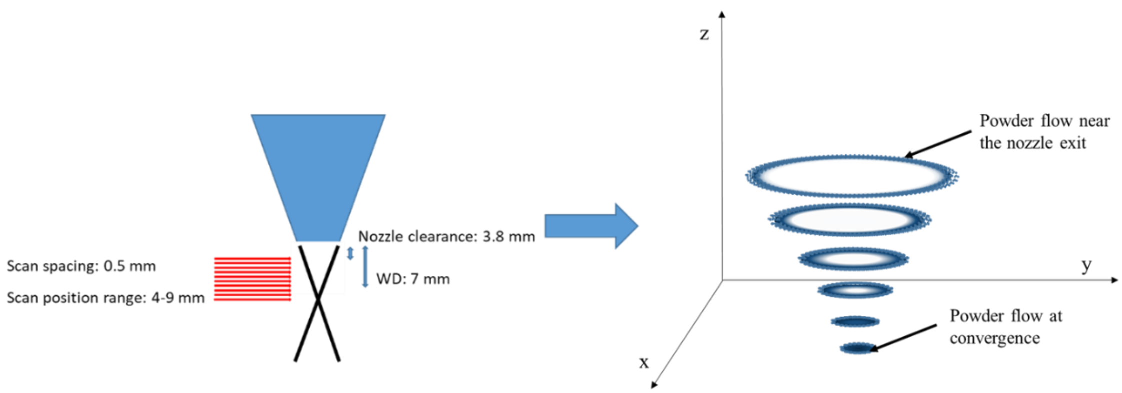

Figure **3-12**: 3D powder flow analysis procedure via 2D scans with 0.5 mm spacing

Utilizing the various methods outlined in this chapter, the ability to demonstrate the PFM system in various use cases can be achieved. The key methods outlined were the determination of a conversion value between powder detections and mass, the minimum sampling time required, and a method to determine mass flow data in 2D and 3D. In chapter 4, the results of the calibration methods and use cases will be detailed in order to demonstrate the accuracy and value of the PFM system for increased powder flow confidence.

Chapter 4

Results

In this chapter, results from PFM calibration, testing, and application to several use cases are presented. First, calibration and correction values are measured to determine the correlation between PFM detections and measured mass flow rate. Next, the effect of integration time is evaluated. Use of the PFM sensor for 2D and 3D characterization of powder flow is demonstrated. In particular, the ability to detect variation in the powder flow due to process parameters, nozzle condition, and in-process phenomenon are assessed. Finally, the utility of the PFM system in detecting nozzle damage and degradation in powder nozzle performance is detailed.

Conversion and Correlation Value

Regardless of the input powder feeder settings, within the measured motor speed of 0.2 to 2 rpm, a strong correlation was observed between PFM detections and measured mass within an identical period of collection. Data collected over 25 test runs is shown in Figure 4-1. A linear fit, with a constant slope of 286724 and zero offset, produced an R^2 value of 0.9977. The slope is equivalent to the number of PFM detections per gram of powder and is used in subsequent analysis within this work. The goodness of fit shows that the PFM system is capable of recording an accurate powder flow rate using the utilized powder (see Case 1) and within the utilized range of powder flow rates.

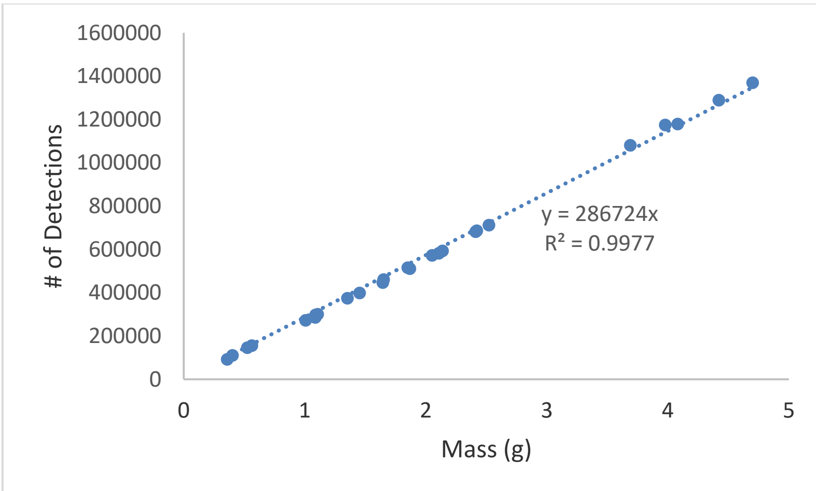

Figure **4-1**: PFM detections vs. scale mass plot and generation of correlation value (slope) and coefficient of determination (R^2) of 4-nozzle deposition head (config. 1).

With the knowledge of the PFM system's capabilities, the experimental determination of a correlation coefficient for the Optomec LENS MR-7 coaxial nozzle was found. Ten tests were conducted at a constant RPM value of 1.2 g/min which also revealed a strong correlation with an R^2 value of 0.9863. A linear fit was observed and a constant slope of 32666 with zero offset. As shown in Figure 4-2, while the actual mass flow rate varied based on each test, the strong correlation further strengths the PFM system's accuracy in recording powder flow rate.

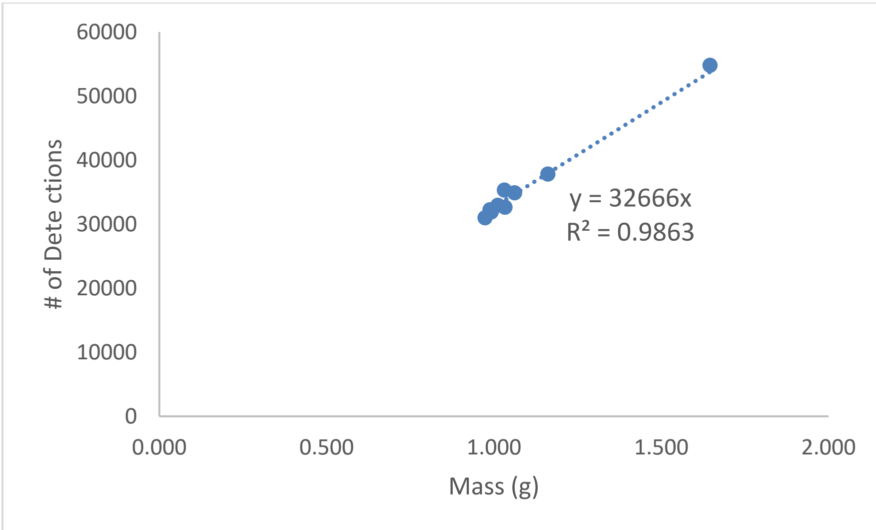

Figure **4-2**: PFM detections vs. scale mass plot and generation of correlation value (slope) and coefficient of determination (R^2) of coaxial nozzle deposition head (config. 4).

Minimum Time Integration

Utilizing the correlation value collected for the 4-nozzle deposition head in the "Correlation and Conversion Value" section, the minimum time integration was determined. PFM sensor data converted into a cumulative mass total overlaid the cumulative mass total recorded by the scale which revealed a strong fit between the two curves, depicted in Figure 4-3. Small artifacts were observed in all samples due to the purge gas flow rate applying additional force to the scale and relieved from the scale after test completion. To avoid the artifacts at the beginning and end of scale measurements, a 10-second region from the center of the PFM and scale data was extracted.

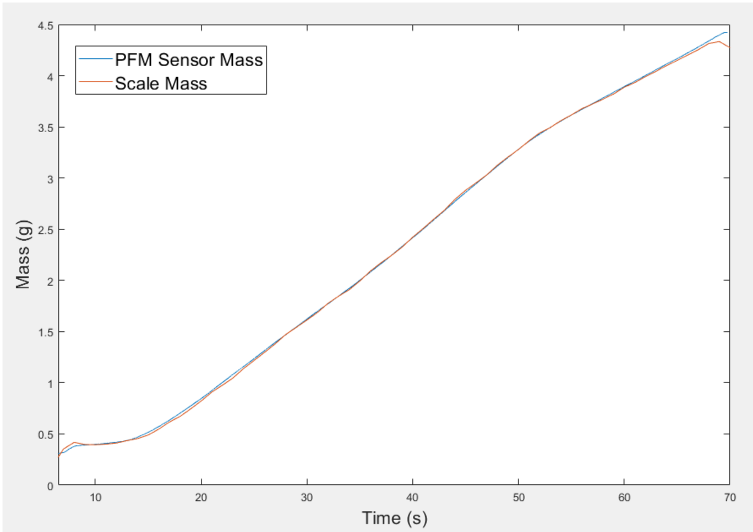

Figure **4-3**: Overlay of PFM cumulative mass and scale recorded mass plots

Taking the derivative of each extracted section of the curve revealed high levels of noise in the PFM data. This occurred due to the high sampling rate of the PFM system as compared to the low sampling rate of the scale. The lower sampling rate of the scale also showed oscillation with an amplitude on the order of 0.03 g—given the ± 0.01 g error associated with scale measurements, this is within the expected range of oscillations around a mean value.

To determine the minimum time integration, time averaging of the PFM data was performed in 0.005 second increments until the PFM data fit within the maximum and minimum rate of change of the scale data; that is, to bring the effective accuracy of the PFM sensor within that of the scale's accuracy. As observed in Figure 4-4, the noise of the PFM data quickly reduced when the minimum time integration required was determined to be 0.015 seconds.

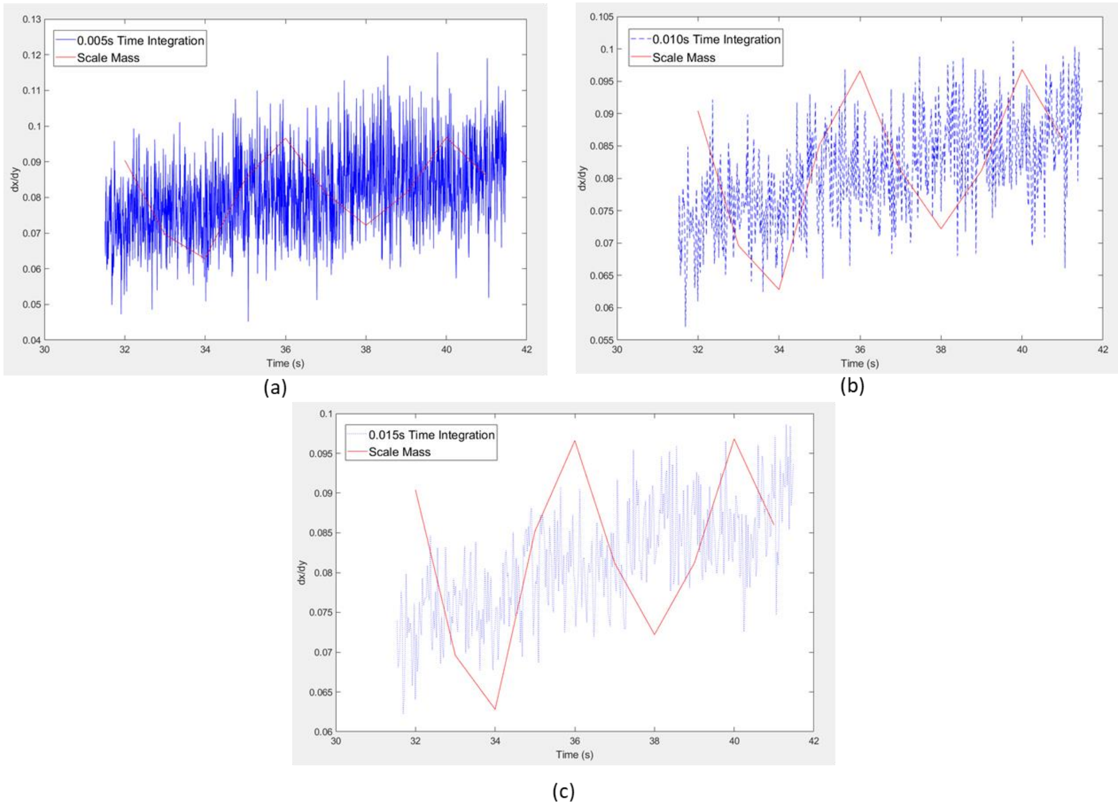

Figure **4-4**: Overlay of rate of change for cumulative scale mass plot and time integration of PFM cumulative data plots at times (a) 50 ms, (b) 100 ms, (c), and 150 ms.

Powder Flow 2D and 3D Analysis

The PFM was used to analyze powder flow under three conditions (see Table 3-2): (1) using a damaged and undamaged coaxial nozzle (3 mm) on a DMG Mori Lasertec 65 DED System, (2) using a damaged coaxial nozzle (1.6 mm) on a DMG Mori Lasertec 65 DED System, and (3) during processing with an Optomec LENS MR7 system equipped with a coaxial nozzle (~1.5 mm) to observe how material (i.e. spatter) buildup upon the nozzle affected powder flow.

Powder Flow from Undamaged Nozzle

The PFM was positioned to measure flow directly underneath a new, undamaged DMG Mori Lasertec 65 3 mm nozzle. The data was represented in two forms. A heatmap was used to qualitatively visualize the flow. Quantitative calculation of an overall mass flow rate of the powder for every 5-second time lapse was used to measure the flow. The heatmap for the chosen location is shown in Figure 4-5, where a uniform powder intensity can be observed.

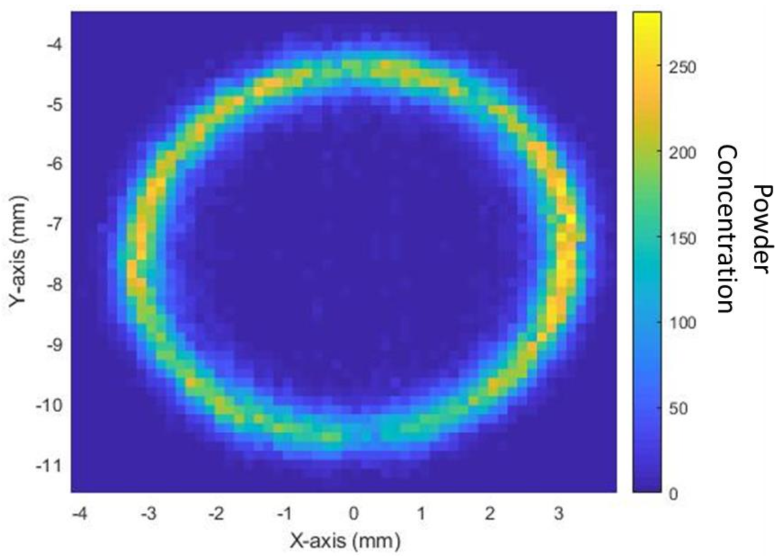

Figure **4-5**: 2D Heatmap of the powder flow generated during PFM data acquisition.

As detailed in Chapter 3, PFM data was analyzed by first converting detections into polar coordinates, shown in Figure 4-6 where every powder particle detected is represented. A best-fit Gaussian distribution applied to the histogram of detection radii can then be determined with an effective powder flow radius (r_{eff}) and an effective width (w_{eff}), where the w_{eff} represents the calculated standard deviation of the Gaussian fit.

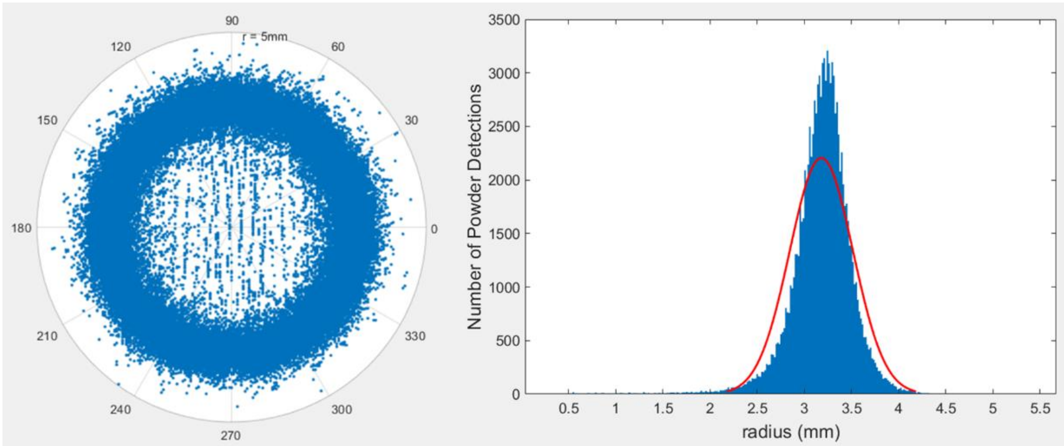

Figure **4-6**: Plot of powder flow at highest plane recorded in polar coordinates and corresponding histogram/Gaussian normal distribution

Splitting the data into four quadrants enabled analysis of the effective powder flow radius (r_{eff}) and effective width (w_{eff}) around the nozzle. The plot shown in Figure 4-7 depicts the plot of the plane directly below the nozzle, where each data point has been grouped into its respective quadrant, as well as a plot of each quadrant's corresponding histogram.

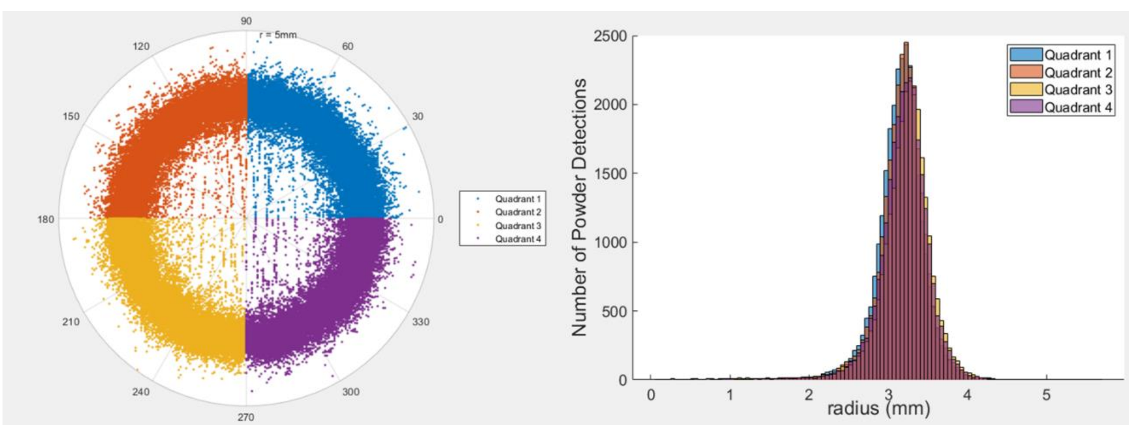

Figure **4-7**: Split flow into quadrants of highest plane recorded and corresponding histograms.

Table 4-2 shows the corresponding r_{eff} and w_{eff} values of each quadrant for the dataset plotted in Figure 4-7. As should be expected with an undamaged, coaxial nozzle, each quadrant shows a very similar r_{eff} and w_{eff} due to the very symmetrical behavior of the powder flow.

Table **4-1**: Effective range and effective width of undamaged 3 mm nozzle on DMG Mori 65

	Quadrant 1	Quadrant 2	Quadrant 3	Quadrant 4
r_{eff}	3.11 mm	3.10 mm	3.26 mm	3.27 mm
w_{eff}	0.42 mm	0.42 mm	0.42 mm	0.42 mm

Effect of Flow Parameters

Variation in powder flow parameter, in particular carrier gas flow rate, was found to affect powder flow. To analyze the difference between nominal carrier gas flow rate (6 lpm) and a reduced carrier flow rate (2 lpm), the powder flow directly below the nozzle orifice as well as at the system's designated working distance were analyzed. A plot comparing flow under nominal (identical to that previously analyzed) and reduced carrier gas flow rate is shown in Figure 4-8. This revealed that for the reduced gas flow rate, the powder particles were more dispersed, which increased in severity as the powder reached the working distance. This correlates with literature [9], where lower carrier gas flow rates can reduce the powder retention at the convergence distance and result in a smaller concentration of powder particles at the laser interaction zone.

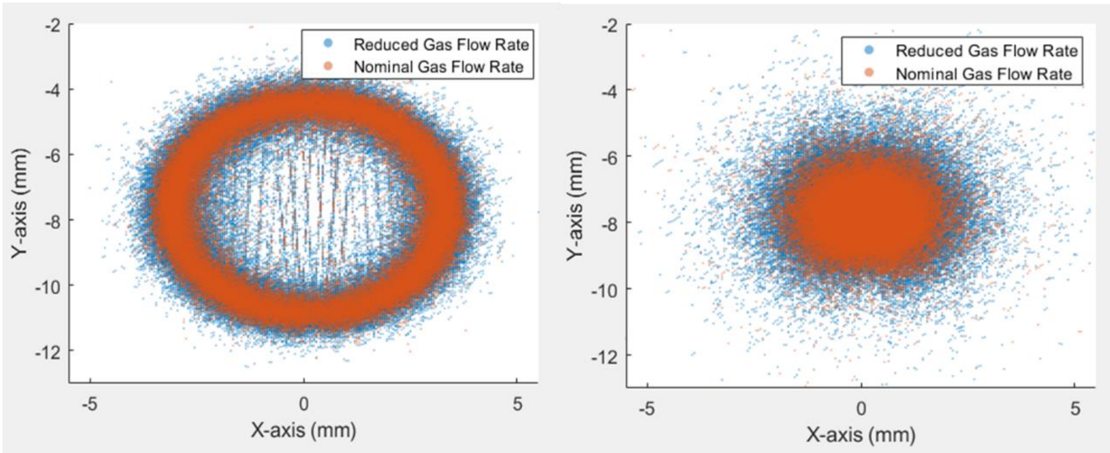

Figure **4-8**: Powder flow rate at highest plane and working distance for varying carrier gas flow rates

Further analyze of the change in effective radius and effective width under nominal and reduced carrier gas flow conditions was measured using percent error $\left(\left|\frac{nominal-reduced}{nominal}\right|\right)$and shown in Table 4-2 and Table 4-3. While effective radius did not increase significantly with a decrease in carrier gas flow, the effective width measured directly below the nozzle orifice and at the working distance did show a large increase. The r_{eff} percent error measured directly underneath the nozzle orifice also showed a much higher error than at the working distance. This is due to the smaller r_{eff} value at the working distance, which causes the changes in the effective radius to result in a higher error value. Overall, this use case shows that both the r_{eff} and w_{eff} values, measured via the PFM, indicate variation in flow geometry and can be used for the detection of gas flow variations.

Table **4-2**: Percent error calculations of r_{eff} and w_{eff} values for the plane directly below the nozzle orifice.

Top Plane	**Nominal r_{eff} (mm)**	**Nominal w_{eff} (mm)**	**Reduced r_{eff} (mm)**	**Reduced w_{eff} (mm)**	**r_{eff} Error (%)**	**w_{eff} Error (%)**
Quadrant 1	3.11	0.42	3.10	0.33	0.32	21.43
Quadrant 2	3.10	0.41	3.09	0.33	0.32	19.51
Quadrant 3	3.26	0.42	3.26	0.36	0.00	14.29
Quadrant 4	3.27	0.42	3.27	0.34	0.00	19.05

Table **4-3**: Percent error calculations of (r_{eff}) and w_{eff} values for the working distance

Working Distance	**Nominal r_{eff} (mm)**	**Nominal w_{eff} (mm)**	**Reduced r_{eff} (mm)**	**Reduced w_{eff} (mm)**	**r_{eff} Error (%)**	**w_{eff} Error (%)**
Quadrant 1	0.93	0.62	0.96	0.68	3.23	9.68
Quadrant 2	0.88	0.59	0.95	0.67	7.95	13.56
Quadrant 3	0.96	0.57	0.98	0.65	2.08	14.04
Quadrant 4	1.00	0.59	0.98	0.64	2.00	8.47

The powder flow shape can also be observed visually by comparing the 3D data for the nominal and reduced carrier gas flow rate. Figure 4-9 shows each 3D plot and the amount of observable powder particle scatter in each. It is apparent that the reduced gas flow rate resulted in a large amount of powder particle scatter and a less uniform powder flow shape.

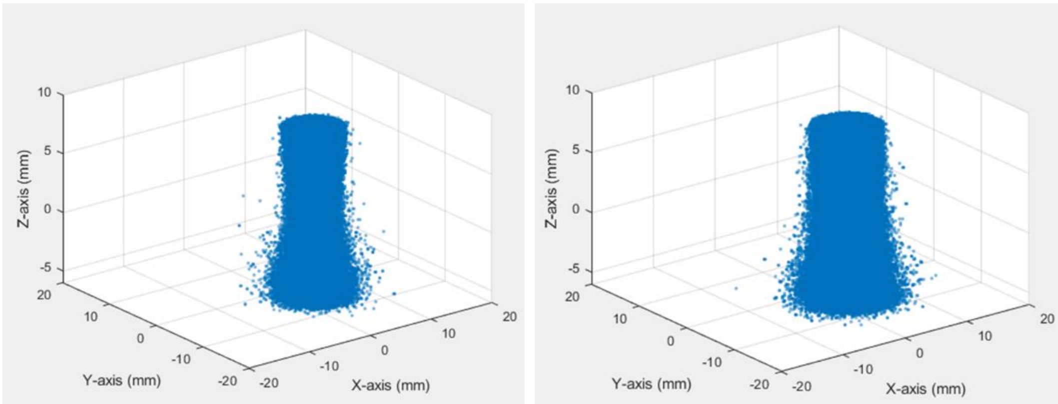

(a) (b)

Figure **4-9**: 3D powder flow shape comparison between (a) nominal (6 lpm) and (b) reduced (2 lpm) gas flow rates

Characterization of Nozzle Damage

On the DMG Mori Lasertec 65, a 3 mm nozzle which was damaged during use, was analyzed to compare its powder flow characteristics against a new, undamaged nozzle used in Configuration 2. The damaged nozzle showed a greater dispersion of powder both directly below the nozzle orifice and at the working distance. As shown in Figure 4-10, the undamaged nozzle had a tight circular pattern while the damaged nozzle had a large amount of powder scattering at each plane. This variation is to be expected with a damaged nozzle, where the shape of the nozzle orifice is warped.

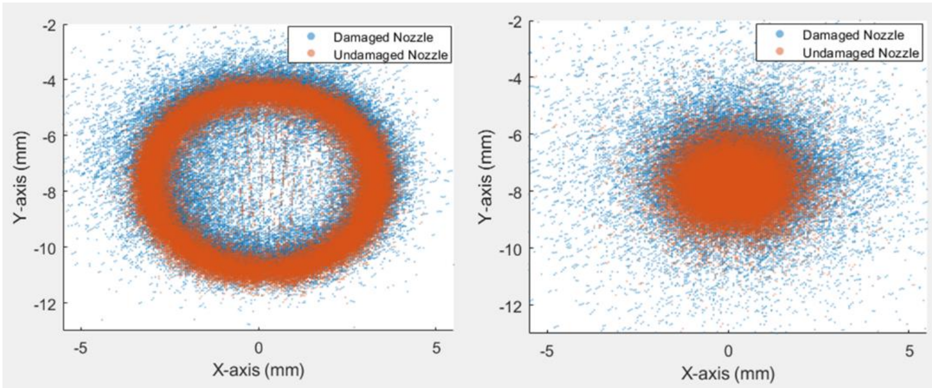

Figure **4-10**: Powder flow rate at highest plane and working distance for a damaged vs. new nozzle

Analyzing the two nozzles' 2D data at the top plane and working distance for their r_{eff} and w_{eff}, plots were created which show the large variation between the two, see Figure 4-11 and Figure 4-12. Directly underneath the orifice of each nozzle (see Figure 4-11) the undamaged nozzle had a relatively flat r_{eff} and w_{eff} value for each quadrant while the damaged nozzle showed significant fluctuations in r_{eff} and a consistently greater w_{eff} .

The reason for this can be observed in Figure 4-10, where nozzle damage caused an increase in the powder particles in quadrants I and II and a decrease in the powder particle presence in quadrants III and IV. However, for each quadrant, w_{eff} increased for the damaged nozzle, indicating a more dispersed flow. At the working distance (see Figure 4-12) a relatively flat r_{eff} and w_{eff} values were observed again while the damaged nozzle showed significant increase in both r_{eff} and w_{eff} values. This is due to the overall scatter observed in Figure 4-10 which increases both of these values significantly.

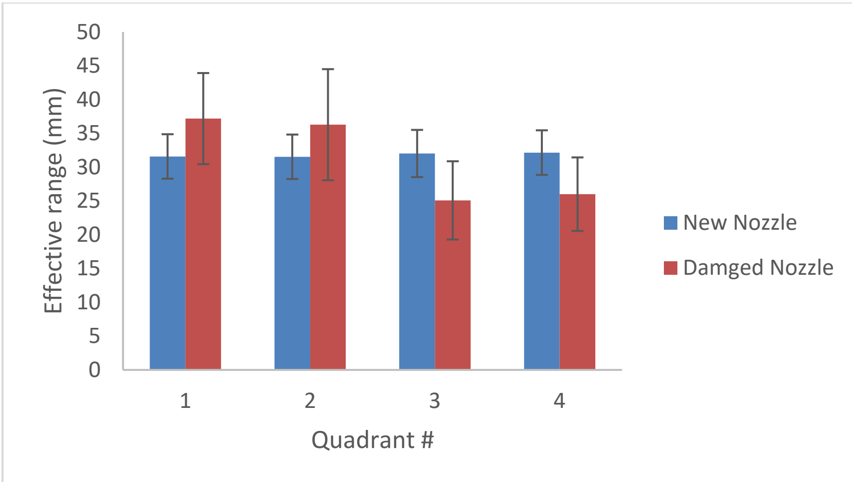

Figure **4-11**: The r_{eff} and w_{eff} values at highest plane for a damaged and undamaged nozzle

At the working distance, an increase in r_{eff} and w_{eff} was observed for all quadrants using the damaged nozzle.

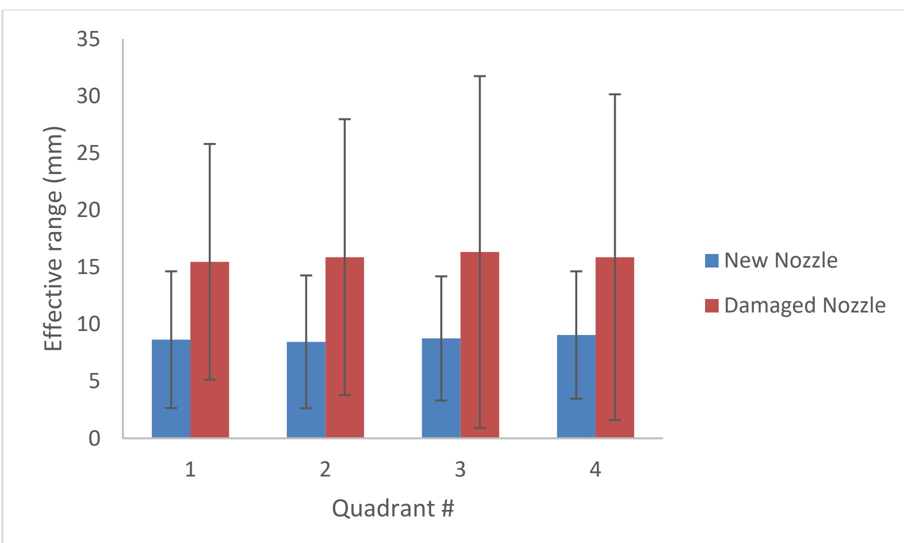

Figure **4-12**: The (r_{eff}) and w_{eff} values at the working distance for a damaged and undamaged nozzle

While the effect of flow disruptions on resulting deposition geometry are outside the scope of this work, it should be noted that flow disruptions are likely to have a significant effect. To illustrate this point, a second significantly-damaged nozzle was used for DED on the DMG Mori Lasertec 65 system, see Configuration 3. PFM data collected directly below the nozzle orifice are shown in Figure 4-12. Deposition with this nozzle resulted in a highly irregular DED track. The resulting track cross-section, shown in Figure 4-13, shows a heat-affected zone (HAZ) with a width of 1985 µm but a deposit (fusion zone) with a width of 975 µm. The width of the HAZ was as expected, indicating no disruption in the energy source, but the fusion zone geometry was irregular and approximately half the expected width, indicating a significant disruption in powder flow, as verified by the PFM heatmap (see Figure 4-14).

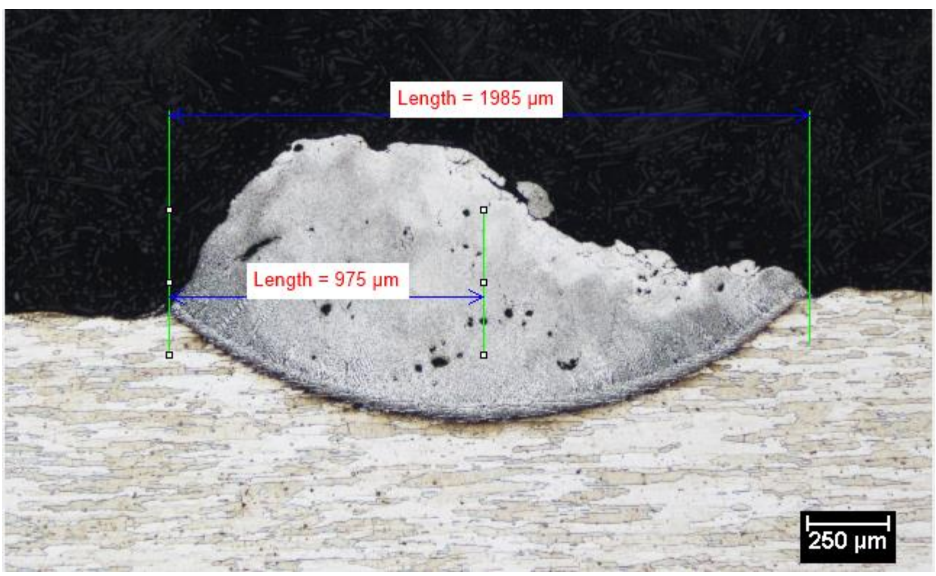

Figure **4-13**: Cross sectional error of a deposit with a damaged nozzle

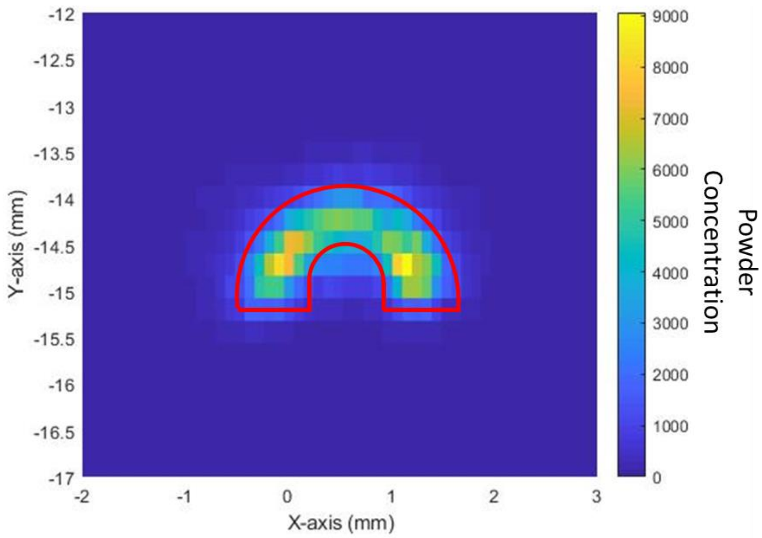

Figure **4-14**: 2D intensity heatmap of damaged nozzle with half of powder flow detected

Detection of Material Build-up

The final use case for the PMF system is to detect the presence of error during a build using an Optomec LENS MR-7 DED system equipped with a damaged ~1.5 mm nozzle. This was achieved through the implementation of the PMF sensor into the build chamber to perform a 3D analysis of the powder flow every two layers. The error that this study focuses on, which is typical of coaxial nozzle DED systems, is the accumulation of material (e.g., sintered powder or spatter) at the orifice of the nozzle. The material accumulation is caused by the buildup of heat at the nozzle orifice and subsequent powder sintering within the nozzle or at its orifice. During deposition, spatter from the laser-interaction zone, may also cause material accumulation. In both cases, this phenomenon can affect the powder flow by blocking the powder from exiting at the location where the material has adhered. For this experiment, only a partially damaged nozzle was available. Thus, the initial flow characteristics, shown in Figure 4-15, and those during material buildup (every two DED layers) were compared.

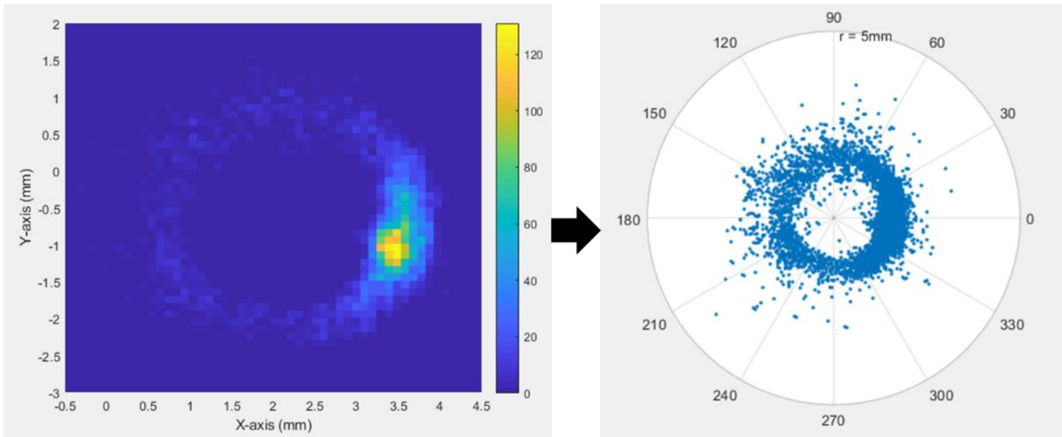

Figure **4-15**: 2D intensity heatmap compared to 2D scatterplot for coaxial nozzle initial condition of powder flow

Inter-layer analysis of the powder flow during a build revealed the increasing effect of spatter accumulation at the nozzle exit onflow. During the build, material began to form on the nozzle after the 14th layer between quadrants II and III. The material continually grew until the flow was catastrophically affected after the 20th layer. Figure 4-16 shows the progression from the original condition to the initial material adherence, until powder flow failure.

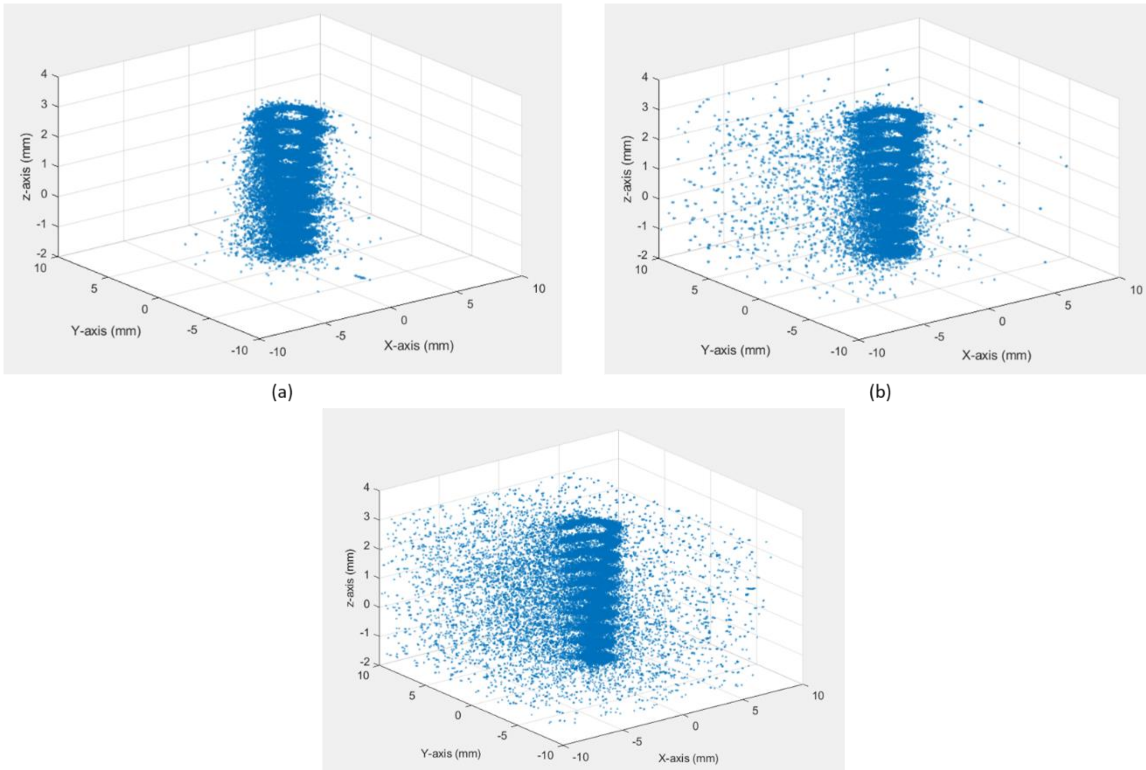

(a) (b)

(c)

Figure **4-16**: 3D powder flow of the (a) 4th layer, (b) 14th layer, and (c) 20th layer of a DED build.

While the 3D visualization (Figure 4-16) reveals a gap that is generated during the material buildup on the nozzle, a 2D slice of the flow after the 20th layer (see Figure 4-17) shows this more clearly. Within quadrants II and III, particularly between 150 and 210 degrees, powder flow was nearly blocked. There was a corresponding increase of powder flow (i.e., a great density of data points) in quadrants I and IV. This increase was even more pronounced at the working distance where the flow in quadrants II and III had been almost completed obstructed as seen in Figure 4-18.

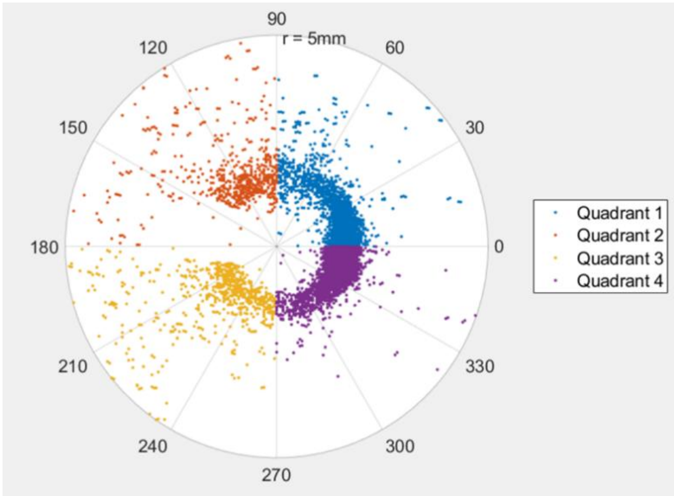

Figure **4-17**: 2D powder flow analysis directly below the nozzle with material buildup interference between Quadrants II and III

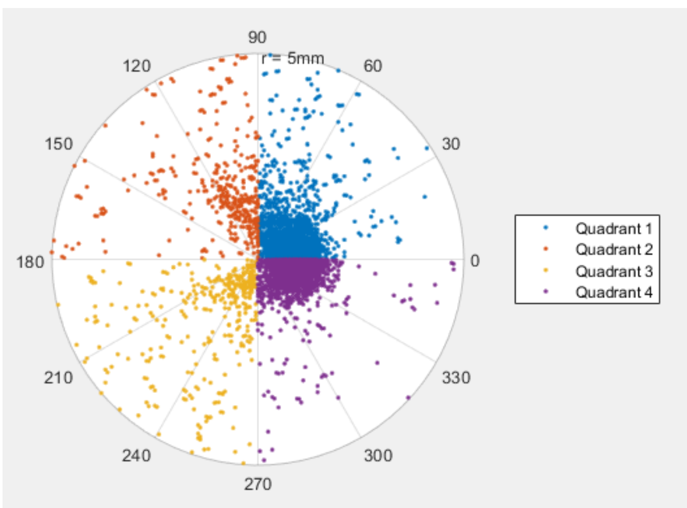

Figure **4-18**: 2D powder flow analysis at the working distance with material buildup interference between Quadrants II and III

Directly below the nozzle orifice, r_{eff} and w_{eff} begin to increase, particularly within quadrants II and III, around the 14^{th} layer of deposition, as shown in Figure 4-18. At this same layer, accumulation of material at the nozzle orifice was visually observed. The effective radius and effective width, measured at the working distance were affected similarly (see Figure 4-19). These increases in, r_{eff} and w_{eff} indicate an initial buildup of material, beginning at the 10th layer, primarily affecting quadrants II and III.

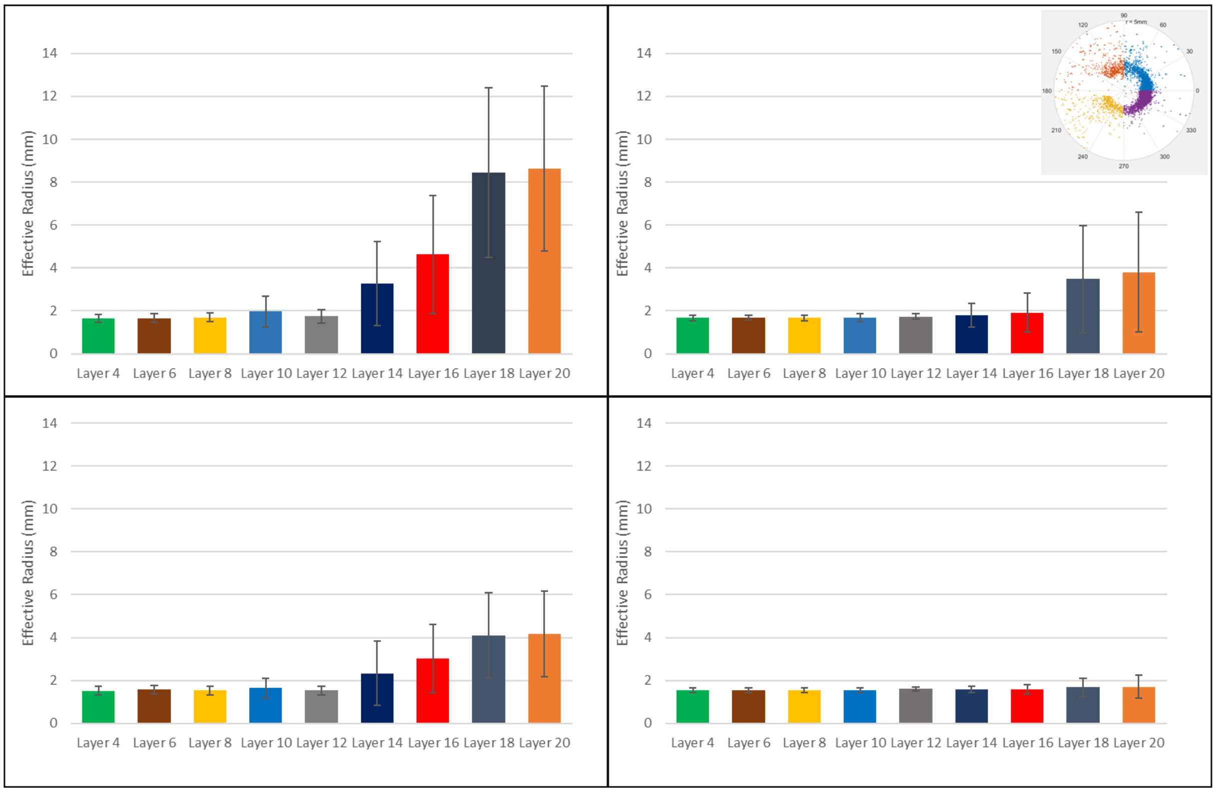

Figure **4-19**: r_{eff} and w_{eff} values directly below the nozzle for each inter-layer data collection in quadrant I (top right), quadrant II (top left), quadrant III (bottom left), and quadrant IV (bottom right)

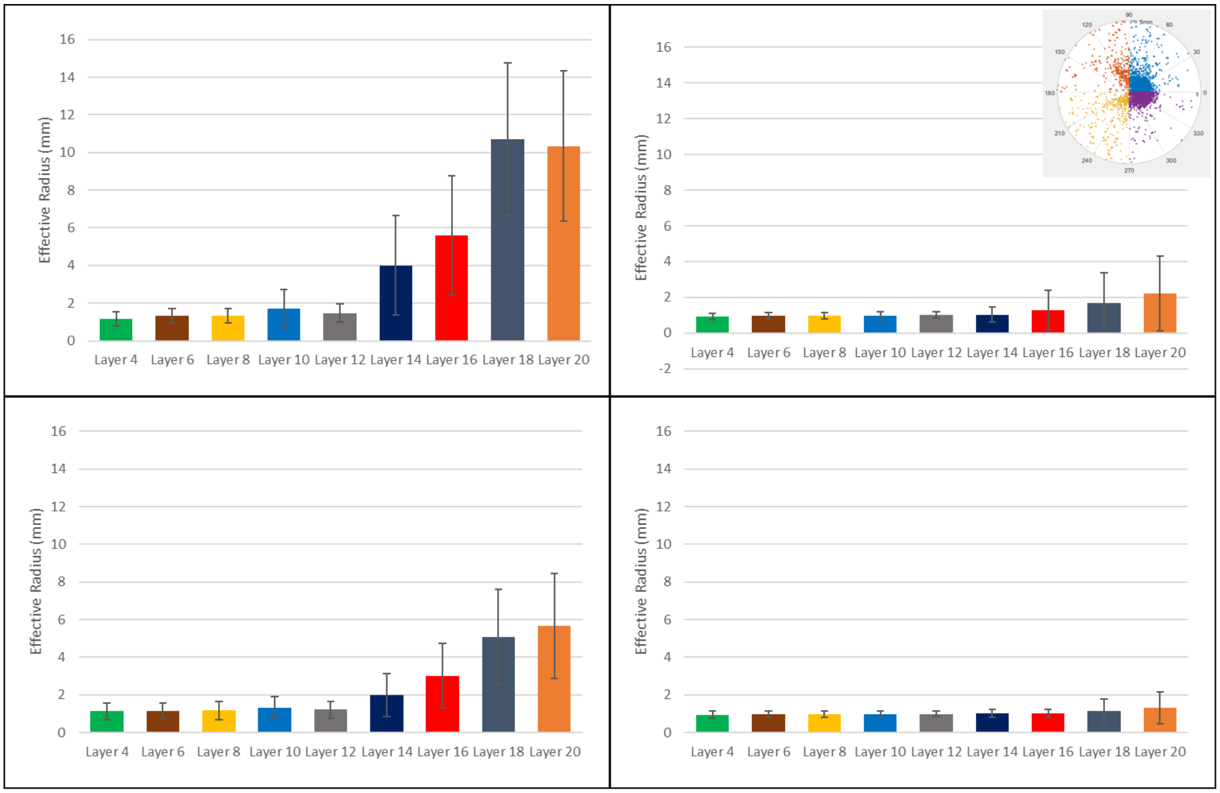

Figure **4-20**: r_{eff} and w_{eff} values at the working distance for each inter-layer data collection in quadrant I (top right), quadrant II (top left), quadrant III (bottom left), and quadrant IV (bottom right)

Assessment of Results

This analysis of the r_{eff} and w_{eff}, together with the visual representations of the data via 2D and 3D plots, show that the PFM system and techniques developed in this study enable assessment of parameter effects, flow disruptions, error, and anomalies. Depicted in each use case, the PFM system was able to analyze the real-time flow characteristics and determine an optimal adjustment, replacement of components, or the emergency stop of a build. When analyzing the corresponding effects of adjusting the gas flow rate, a clear direction to maintain a higher flow rate was determined. After determining the optimal flow characteristics of a nozzle, a damaged nozzle was clearly determined to produce undesirable flow characteristics qualitatively and quantitatively. Finally, the accumulation of material buildup was monitored which revealed the PFM system's ability to determine when a build should emergency stop to take correctional measures, in this case determined to be at layer 10.

Chapter 5

Conclusions

In this study, the development of a robust PFM system was achieved. This system exhibited high accuracy for powder flow rate measurements through extensive experimental validation. The system was tested via multiple use cases, where powder flow characteristics were discerned:

- The effects of varying carrier gas flow rate on the powder flow shape revealed that with a reduction in the carrier gas flow rate, the powder flow became more chaotic. This PFM system showed an increase in effective width (w_{eff}) and effective radius (r_{eff}), indicating a large, irregular powder stream at the working distance.
- Use of a damaged nozzle resulted in disruption of the powder flow and resulted in build error. This analysis further enforced the idea that the increase in w_{eff} as well as the substantial increase in the extensive range revealed error in the powder flow.
- The third use case utilized the information attained from the first two in order to monitor the buildup of material (i.e., spatter) on a nozzle during a build on a DED AM system. This demonstrated the ability to detect error in the flow and take corrective measures to avoid drastic error in the corresponding build.

Through the development of this PFM sensor, the ability to monitor powder flow and determine the presence of error can significantly improve the confidence in parts produced with powder-blown DED AM. In comparison to systems detailed in the literature, which observe the variation in the powder flow in the feed lines, the developed PFM system can quantify variations in the total powder flow rate as well as local variations of the flow between the deposition head the substrate. This represents a significant improvement over the state-of-the-art.

Future work will aim to develop and integrate the developed PFM system and methods onto commercial DED machines. The system will enable reporting flow rates and flow geometry on an inter-layer basis. Analysis may be conducted by assessing the effective radii (r_{eff}) or local flow rate as a function of distance from the deposition head (z) and/or azimuth (θ) on a coaxial nozzle system. Exploration into different distributions, Weibull or Chi-Squared, may increase the accuracy of the analysis at the powder convergence. Further investigation is required to determine the viability of the developed methodology for detecting error in a 4-nozzle DED system as well as an appropriate distribution. Utilizing the minimum time integration determined, a reduced inter-layer data collection methodology can be developed to further reduce the monitoring system's footprint on build time. In summary, using established limits for flow rate and geometry, the system will enable rapid quality measurement, 150 ms integration time, and validation of powder flow, thus enhancing confidence in process quality.

References

[1] T. DebRoy *et al.*, “Scientific, technological and economic issues in metal printing and their solutions,” *Nature Materials,* 2019, doi: https://doi.org/10.1038/s41563-019-0408-2.

[2] I. Gibson, D. Rosen, and B. Stucker, *Additive Manufacturing Technologies*. Boston, MA, USA: Springer, 2010.

[3] N. A. Kistler, A. R. Nassar, E. W. Reutzel, D. J. Corbin, and A. M. Beese, “Effect of directed energy deposition processing parameters on laser deposited Inconel ® 718: External morphology,” Journal of Laser Applications, vol. 29, p. 022005, 2017, doi: http://dx.doi.org/10.2351/1.4979702.

[4] D. Corbin, A. R. Nassar, E. (Ted) Reutzel, A. M. Beese, and P. (Pan) Michaleris, “Effect Of Substrate Thickness And Preheating On The Distortion Of Laser Deposited Ti-6Al-4V,” Journal of Manufacturing Science and Engineering, vol. 140, no. 6, p. 061009, Jan. 2018, doi: 10.1115/1.4038890.

[5] A. Vasinonta, J. L. Beuth, and M. L. Griffith, “Process maps for laser deposition of thin-walled structures,” in Solid Freeform Fabrication Proceedings, 1999, pp. 383–391, Accessed: Dec. 16, 2013. [Online]. Available: http://utwired.engr.utexas.edu/lff/symposium/proceedingsArchive/pubs/Manuscripts/1999/1999-045-Vasinonta.pdf.

[6] J. Choi and Y. Chang, “Characteristics of laser aided direct metal/material deposition process for tool steel,” *International Journal of Machine Tools & Manufacture*, vol. 45, no. 4-5, pp. 597-607, Apr. 2005, doi: 10.1016/j.ijmachtools.2004.08.014.

[7] M. Liu, A. Kumar, S. Bukkapatnam, and M. Kuttolamadom, “A review of the anomalies in directed energy deposition (DED) processes and potential solutions,” *arXiv: Applied Physics*, Nov. 2020.

[8] “A comparison of laser types: CO2, fiber and vanadate lasers.” Trotec. https://www.troteclaser.com/en/faqs/laser-types/ (accessed Jan. 12, 2021).

[9] S. Takemura, R. Koike, Y. Kakinuma, Y. Sato, and Y. Oda, “Design of powder nozzle for high resource efficiency in directed energy deposition based on computational fluid dynamics simulation,” *The International Journal of Advanced Manufacturing Technology*, vol. 105, 4107–4121, Mar. 2019, doi: 10.1007/s00170-019-03552-1.

[10] S. Jhang, Y. Lo, and T. Le, “Systematic modeling approach for analyzing the powder flow and powder energy absorptivity in DED system,” *The International Journal of Advanced Manufacturing Technology*, vol. 105, no. 1, Nov. 2019, doi:10.1007/s00170-019-04441-3.

[11] J. Whiting, A. Springer, and F. Sciammarella, “Real-Time acoustic emission monitoring of powder flow rate for DED,” *Additive Manufacturing*, vol. 23, pp. 312-318, Oct. 2018, doi: 10.1016/j.addma.2018.08.015.

[12] “Metering screw feeders for exact dosing of powders and bulk solids.” Gimat. https://www.gimatengineering.com/powder-feeders (accessed Jan. 12, 2021).

[13] D. M. Keicher, J. W. Love, K. J. Dullea, J. L. Bullen, P. H. Gorman, and M. E. Smith, “Forming Structures From CAD Solid Models”, US Patent 6811744, Apr. 22, 2002.

[14] *9MP Powder Feeder Plasma/Combustion Spraying*, Oerlikon Metco, Pfäffikon, Switzerland, 2018.

[15] S. W. Brown, A. G. Przyjemski, M. B. McPherson, J. H. Steinberg, D. J. Corbin, and E. W. Reutzel, “Insights into powder flow characterization methods for directed energy distribution additive manufacturing systems,” presented at the Solid Freeform Fabrication, Austin, TX, Aug. 2018.

[16] P. Balu, P. Leggett, R. Kovacevic, “Parametric study on a coaxial multi-material powder flow in laser-based powder deposition process,” *Journal of Materials Processing Technology*, vol. 212, no. 7, pp. 1598-1610, July 2012, doi: 10.1016/j.jmatprotec.2012.02.020.

[17] S.Y. Wen, Y.C. Shin, J.Y .Murthy, P.E. Sojka, “Modeling of coaxial powder flow for the laser direct deposition process,” *International Journal of Heat and Mass Transfer*, vol. 52, no. 25-26, pp. 5867-5877, Dec. 2009, doi: 10.1016/j.ijheatmasstransfer.2009.07.018.

[18] X. Guan and Y. F. Zhao, “Numerical modeling of coaxial powder stream in laser-powder-based Directed Energy Deposition process,” *Additive Manufacturing*, vol. 34, Aug. 2020, doi: 10.1016/j.addma.2020.101226.

[19] F. Mazzucato, S. Tusacciu, M. Lai, S. Biamino, M. Lombardi, and A. Valente, “Monitoring approach to evaluate the performances of a new deposition nozzle solution for DED systems,” *Technologies*, vol. 5, no. 2, p. 29, May 2017, doi: 10.3390/technologies5020029.

[20] Z. Liu, H. Zhang, S. Peng, H. Kim, D. Du, and W. Cong, “Analytical modeling and experimental validation of powder stream distribution during Direct Energy Deposition,” *Additive Manufacturing*, vol. 30, Dec. 2019, doi: 10.1016/j.addma.2019.100848.

[21] D. Hu and R. Kovacevic, “Sensing, modeling and control for laser-based additive manufacturing,” *International Journal of Machine Tools & Manufacture*, vol. 43, pp. 51-60, Jan. 2003, doi: 10.1016/S0890-6955(02)00163-3.